This manuscript was accepted and published by ***Energy & Fuels***, a journal of the American Chemical Society. DOI: 10.1021/ef3019222 (http://doi.org/10.1021/ef3019222).

This manuscript was placed into the present public repository with the consent of the Editor of *Energy & Fuels*. Publication data of the final, corrected work:

D. Tapasvi, R. Khalil, G. Várhegyi, Ø. Skreiberg, K.-Q. Tran, M. Grønli:
Kinetic behavior of torrefied biomass in an oxidative environment.
Energy Fuels, 27 (2013) 1050-1060.

The Kinetic Behavior of Torrefied Biomass in an Oxidative Environment

Dhruv Tapasvi,[||] *Roger Khalil,*[‡] *Gábor Várhegyi,*[*,§] *Øyvind Skreiberg*[‡]*, Khanh-Quang Tran,*[||] *and Morten Grønli*[||]

[||]Department of Energy and Process Engineering, Norwegian University of Science and Technology (NTNU), NO-7491 Trondheim, Norway

[‡]SINTEF Energy Research, Postboks 4761 Sluppen, NO-7465 Trondheim, Norway

[§]Institute of Materials and Environmental Chemistry, Research Centre for Natural Sciences, Hungarian Academy of Sciences, PO Box 17, Budapest, Hungary 1525

KEYWORDS Torrefied wood; beech; pine; thermogravimetry; distributed activation energy model; combustion; char burn-off; pyrolysis; kinetic regime.

ABSTRACT. The combustion of four torrefied wood samples and their feedstocks (birch and spruce) was studied at slow heating programs, under well-defined conditions by thermogravimetry (TGA). Particularly low sample masses were employed to avoid the self-heating of the samples due to the huge reaction heat of the combustion. Linear, modulated and constant-reaction rate (CRR) temperature programs were employed in the TGA experiments in gas flows of 5 and 20% O_2. In

this way the kinetics was based on a wide range of experimental conditions. The ratio of the highest and lowest peak maxima was around 50 in the experiments used for the kinetic evaluation. A recent kinetic model of Várhegyi et al. [Energy & Fuels **2012**, *26*, 1323-1335] was employed with modifications. This model consists of two devolatilization reactions and a successive char burn-off reaction. The cellulose decomposition in the presence of oxygen has a self-accelerating (autocatalytic) kinetics. The decomposition of the non-cellulosic parts of the biomass was described by a distributed activation model. The char burn-off was approximated by power-law (n-order) kinetics. Each of these reactions has its own dependence on the oxygen concentration that was expressed by power-law kinetics, too. The complexity of the applied model reflects the complexity of the studied materials. The model contained 15 unknown parameters for a given biomass. Part of these parameters could be assumed common for the six samples without a substantial worsening of the fit quality. This approach increased the average experimental information for an unknown parameter by a factor of 2 and revealed the similarities in the behavior of the different samples.

1. INTRODUCTION

Biomass has been widely recognized as a vital renewable energy source to meet current as well as future energy demands of the world. The extended use of biomass will help to reduce the greenhouse gas emissions and also extends the lifetime of fossil fuel resources. In order to promote biomass usage, various countries have or are trying to establish promising bio-energy policies. The Scandinavian countries take particular efforts in this direction. Sweden for example has set up a goal that 40% of its primary energy supply should come from biomass by 2020.[1] Similarly, Norway formulated a goal of 30% reduction in greenhouse gas emissions before 2020 and certainly, extended biomass usage will help achieve this target.[2]

However, the widespread use of biomass is faced with many challenges linked to the general properties of biomass such as high moisture content, poor grindability, low calorific value and low bulk density. Torrefaction is one of the potential solutions to these problems and it has gained a lot

of research momentum as a biomass pre-treatment process in the last two decades.[3,4] It is essentially a mild pyrolysis process carried out at a temperature between 200 and 300°C in inert atmosphere. During torrefaction the fuel retains most of its energy content. Torrefaction affects mostly the hemicellulose fraction of biomass, but as the process temperature is increased, other biomass components such as cellulose, lignin and extractives are also decomposed. Torrefaction improves the properties of the biomass fuels; among others it reduces the moisture content; increases the energy density and the heating value; changes the hygroscopic behavior of the raw biomass into a hydrophobic behavior, and enhances grindability.[3-5]

Several torrefaction studies are available in the literature. Most of these studies have focused on characterizing torrefied products, evaluating product yields and product properties such as grindability, particle size distribution, and hydrophobicity from various biomass materials such as woods, agricultural residues and energy crops.[3-5] However, as the eventual use of biomass fuel is utilization in thermo-chemical processes such as combustion, gasification and pyrolysis, the actual test of torrefaction is how it affects the behavior of biomass in these processes. So far, only a few studies have attempted to analyze the reactivity of torrefied products in these processes and only limited information is available in this field.[6-14] For combustion, being the main process option for the use of biomass, the understanding of the behavior of torrefied biomass under oxidative conditions should be a priority. The present work aims at studying the combustion process under kinetic control and providing a background for future kinetic sub-models. As thermogravimetric analysis (TGA) is a proven method to collect basic information on the partial processes and reaction kinetics of the thermal degradation of biomass materials, it was chosen for this study. With its high precision and well-controlled experimental conditions, TGA is a useful tool for studying devolatilization and combustion in the kinetic regime.[15,16] However, TGA can be employed only at relatively low heating rates as the true temperature of the samples becomes unknown at high heating rates. Accordingly the results of the TGA studies cannot be utilized directly in the modeling of industrial combustors; they serve as basic research to direct further development in the field.

Among the previous studies, Bridgeman et al.[13], Arias et al.[14], Jones et al.[10] and Broström et al.[12] have utilized TGA to evaluate the combustion reactivity of torrefied samples. No kinetic analysis was performed by Bridgeman et al.[13] Arias et al.[14] divided the TGA experiments into a low and a high temperature stage (below and above ca. 400°C, respectively) and described both stages by first order kinetics. Jones et al.[10] performed TGA experiments on chars that were prepared from torrefied biomass samples, and applied a first order reaction model to deduce kinetic parameters for the char reactivity under oxidative conditions. They observed that the chars from the torrefied samples had lower reactivity than the chars produced from raw samples, but they had higher reactivity than the chars produced from coal. In a later study, Broström et al.[12] provided a detailed kinetic model for the devolatilization and oxidative kinetics of torrefied Norwegian spruce wood. For the devolatilization, measured curves were predicted by three parallel reaction mechanisms corresponding approximately to the three main wood components: hemicellulose, cellulose and lignin. In the presence of oxygen, two additional reactions for the char devolatilization and combustion were included.

The present work continues the efforts of Broström et al.[12] to establish a detailed model for the oxidation kinetics with the following extensions:

(i) Broström et al.[12] used TGA experiments with heating rates 2.5, 5 and 10°C/min at one oxygen concentration on samples prepared from one feedstock (spruce). The TGA experiments of the present work cover a wider set of experimental conditions, as it will be outlined in Section 2.2, and the study is based on two feedstocks: a deciduous and an evergreen species (birch and spruce). The presented kinetic model is based on the least squares evaluation of 36 experiments.

(ii) Broström et al.[12] employed a kinetic model built from n-order independent parallel reactions. In the present work a more complex model is used[17] which tries to reflect better the real complexity of the biomass combustion. The model itself is outlined in Sections 3.2 and 3.3, below. We believe that the fast development of both software and hardware will make it possible to employ the more complex models, too, in practical calculations.

2. SAMPLES AND METHODS

2.1 Sample Characterization and Preparation. The samples were composed of two wood types; birch and spruce, which are commonly available in Norway. Sample particle sizes of 10 mm cubes from both feedstocks were torrefied in a batch reactor (macro-TGA). The details of the torrefaction process were presented in a recent work.[5] The samples were heated at a heating rate of 5º C/min up to either 225 or 275 ºC. Samples with a 60 min holdup time at the torrefaction temperature were used in this kinetic study. Fine grinding of the torrefied samples was performed in a cutting mill equipped with 1 mm bottom sieve. The powder samples were afterwards sieved with a series of sieves of mesh sizes 1 mm, 500 µm, 180 µm, 125 µm and 63 µm in a vibrating sieving machine. The particles belonging to the size 63 – 125 µm were used for the kinetic study. In all, 6 samples were prepared for this study, 4 torrefied samples and the 2 raw fuels. The torrefaction conditions under which the samples were generated, along with the naming convention for these, are presented in Table 1. Table 2 shows the ultimate and proximate analysis of the samples.

Table 1: The samples used for the kinetic modeling

Name	Sample	Torrefaction temperature [ºC]
B --	Birch	none
B225	Birch	225
B275	Birch	275
S --	Spruce	none
S225	Spruce	225
S275	Spruce	275

Table 2: Proximate and ultimate analysis of the samples[a]

Sample	Proximate analysis			Ultimate analysis					
	VM	fC	Ash	C	H	O	N	S	HHV[b]
B --	89.4	10.4	0.2	48.62	6.34	44.9	0.09	< 0.05	19.80
B225	86.4	13.2	0.4	49.90	5.98	44.00	0.10	< 0.05	19.90
B275	77.7	21.9	0.4	54.16	5.65	40.00	0.12	< 0.05	21.40
S --	86.3	13.4	0.2	50.1	6.36	43.52	0.07	< 0.05	20.45
S225	84.0	15.8	0.2	50.97	6.15	42.76	0.07	< 0.05	20.62
S275	75.7	24.2	0.2	55.33	5.73	38.81	0.09	< 0.05	22.05

[a] % (m/m), dry basis. [b] MJ/kg

2.2 Experimental Setup and Procedure. The reactivity studies were conducted in a Q5000 IR analyzer from TA instruments which has a sensitivity of 0.1 µg. 5% v/v and 20% v/v oxygen-nitrogen mixtures were used as purge gas with a gas flow of 100 mL/min. Sample masses of 0.5 mg or less were used to avoid self-heating of the samples due to the high reaction heat. Each sample was analyzed with three different heating programs, as shown in Figure 1:

(i) 10°C/min linear T(t);

(ii) modulated T(t), where sinus waves with 5°C amplitudes and 200 s wavelength were superposed on a slow, 2°C/min linear;

(iii) "constant reaction rate" (CRR) T(t), when the employed equipment regulated the heating of the samples so that the reaction rate would oscillate around a preset limit.[18] The CRR experiments aimed at getting very low mass-loss rates in the whole domain of the reaction. The DTG peak maxima of the CRR experiments varied between 0.04 and 0.07 µg/s. This interval corresponds to rates between 0.8×10^{-4} and 1.3×10^{-4} s^{-1} after normalization by the initial dry sample mass. The T(t) program for a CRR experiment obviously depends on the behavior of the given sample. Figure 1 shows four of the CRR T(t) programs of the present study.

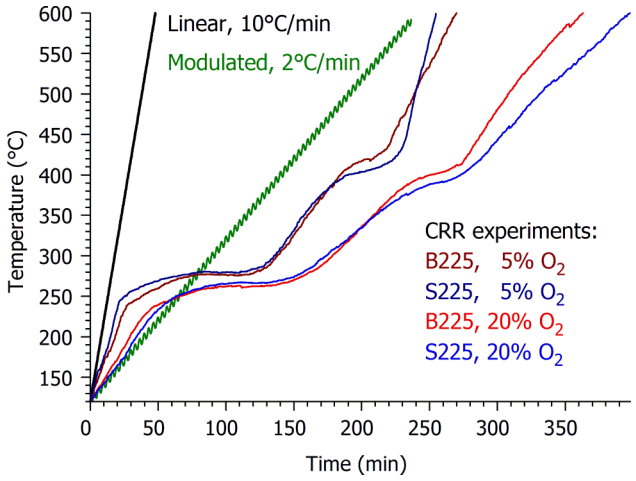

Figure 1. Temperature programs used in the TGA experiments. Note that each of the twelve constant heating rate experiments has different T(t); this figure shows four of them.

The modulated and CRR temperature programs were employed to increase the information content of the data, as outlined in earlier work.[19,20] From one point of view, the linear T(t) experiments with different heating rates are rather similar to each other, hence their information content is limited.[19] On the other hand, an acceptable kinetic model should describe well the experiments at any T(t), including the highly irregular CRR temperature programs, too.[20]

2.3. Numerical Methods. Fortran 95 and C++programs were employed for the numerical calculations and for graphics handling, respectively. The employed numerical methods have been described in details earlier.[21] The kinetic evaluation was based on the least squares evaluation of the $-dm^{obs}/dt$ curves, where m^{obs} is the sample mass normalized by the initial dry sample mass. The method[22] used for the determination of $-dm^{obs}/dt$ does not introduce considerable systematic errors into the least squares kinetic evaluation of experimental results.[23] The model was solved numerically along the empirical temperature – time functions. The model parameters were determined by nonlinear least squares minimization, as outlined in Sections 3.1 and 3.4. The calculations were carried out on a desktop computer equipped with a 3.4GHz Intel Core i7 processor, under Windows. The run times varied between 10 minutes to 10 hours, depending on the initial guess of the parameters in the nonlinear least squares minimization. The calculation of one theoretical DTG curve by the model outlined in Section 3.3 requires 23 μs on average without

parallel computation. With the use of the four cores of the processor one can calculate one million theoretical curves in 96 minutes.

3. RESULTS AND DISCUSSION

3.1. Evaluation by the Method of Least Squares and Characterization of the Fit Quality.

The kinetic evaluation is carried out by the method of least squares. Such values are searched for the unknown model parameters that minimize the following objective function:

$$o.f. = \sum_{k=1}^{N_{exper}} \sum_{i=1}^{N_k} \frac{\left[\left(\frac{dm}{dt}\right)_k^{obs}(t_i) - \left(\frac{dm}{dt}\right)_k^{calc}(t_i)\right]^2}{N_k h_k^2} \quad (1)$$

Here N_{exper} is the number of experiments evaluated together; its value in the present work is either 6 or 36, as outlined later. The division by h_k^2 serves to counterbalance the high magnitude differences. Traditionally h_k is the highest observed value of the given experiment.[24] The normalization by the highest observed values in the least squares sum assumes implicitly that the relative precision is roughly the same for the different experiments. This assumption has proved to be useful in numerous works on non-isothermal kinetics since 1993.[24] Among others, the antecedents of the present work also used it.[17,20,21] However, the magnitude differences were very high in the present work. The peak maxima of the CRR experiments scattered around a very low value, 1×10^{-4} s^{-1}, while the peak maxima of the 10°C/min experiments were roughly 30 times higher. The ratio of the highest and lowest peak maxima was around 50 in the given set of the experiments. Test calculations showed that one cannot assume approximately equal relative precisions at such high magnitude differences. No information was available on the absolute and relative precision of the *-dm/dt* values in the CRR experiments, hence, the choice of the h_k of the CRR experiments could not be based on theoretical considerations. An arbitrary $h_k=5\times10^{-4}$ s^{-1} value was used for the CRR experiments which is ca. 5 times higher than their peak maxima. The fit qualities obtained in this way will be discussed in Section 3.4. The peak maxima of the 10°C/min linear T(t) experiments and the 2°C/min modulated experiments were much higher, around 33×10^{-4}

and 9×10^{-4} s^{-1}, respectively, hence their peak maxima could be used as h_k values, in the usual way. The fit qualities obtained in this way will be shown in details in Section 3.5 and in the Supporting Information.

The obtained fit quality can be characterized separately for each of the experiments evaluated together. The deviation between the observed and calculated DTG values of a given experiment is given as a root mean square (rms):

$$dev_k\,(\mu g/s) = \left\{ N_k^{-1} \sum_{i=1}^{N_k} \left[\left(\frac{dG}{dt}\right)_k^{obs}(t_i) - \left(\frac{dG}{dt}\right)_k^{calc}(t_i) \right]^2 \right\}^{½} \qquad (2)$$

Here subscript k indicates the experiments of the series evaluated; t_i denotes the time values in which the discrete experimental values were taken; N_k is the number of the t_i points in a given experiment and G is the TGA signal without normalization in unit µg.

The deviations defined by eq. (2) can also be expressed as percent of the peak maximum, getting in this way a sort of relative deviation:

$$rel.dev_k\,(\%) = 100\; dev_k \,/\, \max\left(\frac{dG}{dt}\right)_k^{obs} \qquad (3a)$$

The same relative deviations can obviously calculated from $-dm^{obs}/dt$ values, too, because the G and m values differ only by a constant divisor:

$$rel.dev_k\,(\%) = 100 \left\{ N_k^{-1} \sum_{i=1}^{N_k} \left[\left(\frac{dm}{dt}\right)_k^{obs}(t_i) - \left(\frac{dm}{dt}\right)_k^{calc}(t_i) \right]^2 \right\} \Big/ \max\left(\frac{dm}{dt}\right)_k^{obs} \qquad (3b)$$

In the tables of the present work the magnitude of the objective function will be characterized by $100\sqrt{o.f.}$ because this quantity is related to the relative deviations by eq. 3b. If all h_k were equal to the corresponding peak maxima, $100\sqrt{o.f.}$ would be equal to the root mean square formed from the relative deviations of the evaluated experiments.

3.2. Four Main Reactions that are Described by Three Pseudo-components. Figure 2 compares the behavior of the samples at 10°C/min heating rate, in 20% oxygen. As in a previous

work,[17], the DTG curves of the untreated samples (green lines), can be interpreted as the results of four main reactions that partly overlap each other:

(i) the decomposition of the hemicellulose and other thermally labile parts of the sample that dominate the DTG approximately between 200 and 300°C;

(ii) the oxidative decomposition of the cellulose component which produces a sharper peak with a maximum around 335°C;

(iii) a flat section which due to the high temperature end of the lignin decomposition and the slow carbonization and other reactions of the formed char; these reactions dominate the DTG approximately between 360 and 430°C;

(iv) and the char burn-off which result in a peak around 460°C.

Earlier works have shown that reactions (i) and (iii) can be described by the same distributed activation energy model,[17,23,25] as outlined in the next section.

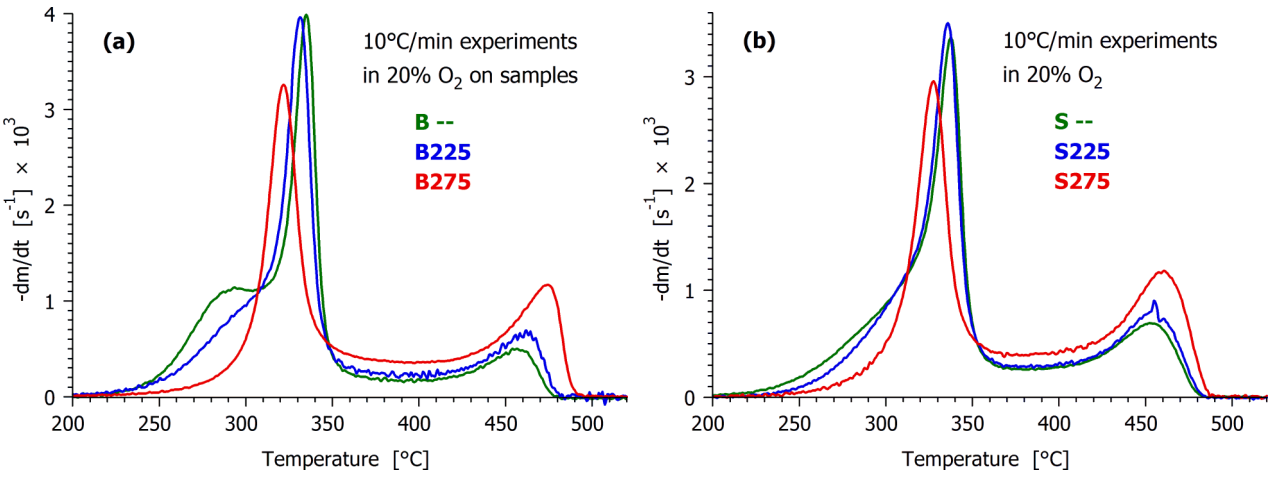

Figure 2. Comparison of the experiments at 10°C/min heating rate, in 20% oxygen

The inorganic components are distributed in various forms in the woody biomass.[26] The ash formation includes chemical reactions as well as the physical agglomeration of the inorganic particles after the burn-off of the organic constituents. The present samples contain only a low amount of mineral matter (0.2 – 0.4%), hence it is possible to neglect the ash-formation reactions. However, this would reduce the future applicability potential of the model. As an alternate solution, the parameter connected to the ash formation will be determined from the total ash of the proximate

analysis, as outlined in the next section. In this way the inclusion of a global ash formation reaction will not increase the number of the unknown parameters in the least squares procedure. From a computational point of view the ash formation rates are proportional to the char burn-off rates; hence their calculation does not require any extra effort.

3.3. The Employed Model. As mentioned in the Introduction, the model of wood combustion is employed from a recent work,[17] except a minor change in the description of the cellulose part of the samples. All masses in the treatment are normalized by the initial sample mass. The normalized amounts of the unreacted part of the sample, char and ash will be denoted by m_{ur}, m_{char} and m_{ash}, respectively. As the reactions proceed, m_{ur} decreases from 1 to 0 because no unreacted biomass remains at the end. m_{char} is zero at the beginning of an experiment. It reaches a maximum as the char forms and converges to zero again as the char burns off. m^{calc} is the sum of the normalized masses of the solid components:

$$m^{calc}(t) = m_{ur}(t) + m_{char}(t) + m_{ash}(t) \tag{4a}$$

$$\frac{dm^{calc}}{dt} = \frac{dm_{ur}}{dt} + \frac{dm_{char}}{dt} + \frac{dm_{ash}}{dt} \tag{4b}$$

The unreacted part of the sample, m_{ur} will be regarded as the sum of the cellulose component and the rest of the sample. The models for pyrolysis kinetics are usually written for variables that run from 0 to 1; accordingly we shall use a reacted fraction for cellulose, $\alpha_{cell}(t)$, and another reacted fraction, $\alpha_{other}(t)$, for the other components of the biomass. The corresponding boundary conditions are $\alpha_{cell}(0)=0$, $\alpha_{cell}(\infty)=1$, $\alpha_{other}(0)=0$ and $\alpha_{other}(\infty)=1$. $m_{ur}(t)$ is the weighted sum of its two constituents with weight factors c_{cell} and c_{other}:

$$m_{ur}(t) = c_{cell}\,[1-\alpha_{cell}(t)] + c_{other}\,[1-\alpha_{other}(t)] \tag{5a}$$

$$-\frac{dm_{ur}}{dt} = c_{cell}\frac{d\alpha_{cell}}{dt} + c_{other}\frac{d\alpha_{other}}{dt} \tag{5b}$$

At t=0 eq. 5a reduces to

$$1 = c_{cell} + c_{other} \tag{5c}$$

The char burn-off will be described by power-law kinetics where the reaction rate is n_{char} order with respect to m_{char} and ν_{char} order with respect to the oxygen concentration, C_{O_2}. Accordingly the char burn-off rate is approximated as

$$\textit{char burn-off rate} = A_{char} C_{O_2}^{\nu_{char}} \exp(-\frac{E_{char}}{RT})\, m_{char}^{n_{char}} \quad (6)$$

Both the cellulose and the non-cellulosic parts of the biomass form char. The corresponding char yields are denoted by $y_{cell.char}$ and y_{other_char}, respectively, which are dimensionless quantities. The char is formed from the biomass decomposition and consumed by the burn-off, hence

$$\frac{dm_{char}}{dt} = c_{cell}\frac{d\alpha_{cell}}{dt} y_{cell.char} + c_{other}\frac{d\alpha_{other}}{dt} y_{other\_char} - A_{char} C_{O_2}^{\nu_{char}} \exp(-\frac{E_{char}}{RT})\, m_{char}^{n_{char}} \quad (7)$$

The ash is formed by the char burn-off reaction with a yield of y_{ash}:

$$\frac{dm_{ash}}{dt} = A_{char} C_{O_2}^{\nu_{char}} \exp(-\frac{E_{char}}{RT})\, m_{char}^{n_{char}}\, y_{ash} \quad (8)$$

Note that a dimensionless C_{O_2} concentration is needed in the kinetic equations. Otherwise the dimension of the preexponential factor should depend on ν_{char} in order to get dm_{char}/dt and dm_{ash}/dt in unit s^{-1}.

In inert atmosphere, under the conditions of thermal analysis the cellulose decomposition is usually regarded to have approximately first order kinetics, though more complex models are also employed. Among others, the use of self-accelerating kinetics has been suggested.[27,28] In the presence of oxygen the cellulose decomposition was found to be a self-accelerating reaction by Várhegyi et al., too.[17] The self-accelerating reactions can typically be described by an equation of type

$$\frac{d\alpha_{cell}}{dt} = A_{cell} C_{O_2}^{\nu_{cell}} \exp(-\frac{E_{cell}}{RT})\, f(\alpha_{cell}) \quad (9)$$

where f is a function capable of expressing self-acceleration. The mathematical unambiguity requires a normalization for $f(\alpha_{cell})$ because f functions differing only in constant multipliers are equivalent in eq. 9 (parameter A_{cell} can compensate any multipliers of f). As a normalization, we require that the maximum of f be 1. $f(\alpha_{cell})$ is approximated formally by

$$f(\alpha_{cell}) \cong normfactor\,(1-\alpha_{cell})^{n_{cell}}\,(\alpha_{cell}+z) \qquad (10)$$

where n_{cell} and z are model parameters and *normfactor* ensures that max f=1. Parameters n_{cell} and z do not have separate physical meaning; together however they determine the shape of f, and, in this way, the self-accelerating capabilities of the model. Eq. 10 is a slightly simplified version of an earlier approximation that has been employed to different self-accelerating reactions.[29,30,17] These earlier works employed an exponent on factor (α_{cell}+z); the omission of this parameter did not affect the fit quality in the present study. A differentiation of eq. 10 by α_{cell} yields that $f(\alpha_{cell})$ reaches its maximum at

$$\alpha_{cell} = (1-n_{cell}z)/(n_{cell}+1) \qquad (11)$$

When eq. 11 gives a negative value, $f(\alpha_{cell})$ is monotonously decreasing in the [0,1] interval. In the present work, however, the maximum of $f(\alpha_{cell})$ proved to be around 0.4 – 0.5. The *normfactor* in eq. 10 is the maximum of $(1-\alpha_{cell})^{n_{cell}}\,(\alpha_{cell}+z)$ in the [0,1] interval, hence its value can be immediately calculated by substituting the α_{cell} value from eq. 11.

The oxidative decomposition of the non-cellulosic part of the sample is described by a distributed activation energy model for reasons as follow. This pseudocomponent includes the decomposition of the extractives, hemicelluloses, and lignin. There is a high number of different reactive species here. The differences in their reactivity are described by different activation energies. To keep the number of unknown model parameters low, the activation energies in this pseudo-component are assumed to have a distribution function. The usual Gaussian distribution function is employed, by an E_0 mean and σ width. The effect of oxygen is described by a power function, $C_{O_2}^{\nu_{other}}$. The reacted fraction of this pseudo-component, α_{other} is calculated by the same high-precision numerical methods that were used in earlier works.[31,17,20,21,23] Note that the term $A_{other}C_{O_2}^{\nu_{other}}$ is a constant multiplier during the numerical solution for a given experiment.

Parameter y_{ash} expresses the ash yield of the char burn-off. In the present work y_{ash} is determined from the total ash obtained by proximate analysis. This latter will be used as a dimensionless ratio,

m_{ash}^{anal}, which is equal to the hundredth of the corresponding percent value in Table 2. The overall ash yield of the model is forced to be equal to m_{ash}^{anal} by equation

$$(c_{cell}\, y_{cell.char} + c_{other}\, y_{other\_char})\, y_{ash} = m_{ash}^{anal} \quad (12)$$

In this way y_{ash} can be eliminated from the model because it can be expressed as a function of m_{ash}^{anal}, y_{other_char} and c_{cell} by equations 12 and 5c.

3.4. Evaluation by Assuming Common Parameters. The model outlined above has 16 unknown parameters for each sample, as follows:

A_{cell}, ν_{cell}, E_{cell}, z, n_{cell}, $y_{cell.char}$, c_{cell} (cellulose decomposition);

A_{other}, ν_{other}, E_0, σ, y_{other_char} (the decomposition of the non-cellulosic parts of the sample; here c_{other}=1-c_{cell} due to eq. 5c);

A_{char}, ν_{char}, E_{char}, and n_{char} (char burn-off).

It turned out during the evaluation that there is a strong compensation effect between parameters $y_{cell.char}$, c_{cell} and y_{other_char}. Practically any $y_{cell.char}$ value can be selected between 0 and ca. 0.2 because c_{cell} and y_{other_char} can compensate its effect so that neither the fit quality nor the rest of the parameters are affected. The Appendix at the end of the article clarifies the problem in detail. As explained there, the physical meaning of the effect is connected to the temperature difference between the devolatilization and the char burn-off. As the figures of the next section and the Supporting Information show, the cellulose decomposition terminates before the start of the char burn-off. If the value of $y_{cell.char}$ is altered, c_{cell} and y_{other_char} can be changed so that the amount of char formed till the start of the char combustion would not change. To overcome this problem, all of the results will be reported at $\boldsymbol{y_{cell.char}}$ **= 0.07** which was the mean value of the cellulose experiments of eight European laboratories in a round-robin work.[32] It is important to emphasise that this choice affect only c_{cell} and y_{other_char} in the tables. Anything else in the tables and in the figures is the same as it were with an assumption of another $y_{cell.char}$ value between 0 and 0.2. (This

was carefully checked; all calculations of the present paper were carried out with more than one $y_{cell.char}$ value.) In this way the number of unknown parameters reduces to 15.

The remaining 15 unknown parameters of the model can be determined by the least squares evaluation of the six experiments of a given sample. In this approach there are 2.5 unknown parameters for one TGA experiment. If all of the parameters are assumed to depend on the sample type then the 6 samples together have 6×15=90 unknown parameters. The total number of the unknown parameters for the six samples will be denoted by N_{param}. There are 36 TGA experiments for the determination of the N_{param} unknown parameters.

If part of the model parameters is assumed to be common for all samples, two benefits can be achieved:

(i) The common parameters will indicate the similarities in the kinetic behavior of the samples;

(ii) Less unknown parameters are derived from the given amount of experimental information (i.e. a given parameter value is based on more experimental information). This helps to eliminate the usual ill-definition (compensation effect) problems of the non-isothermal kinetics. The compensation effects between A and E or A, E and n are well known in the literature of the non-isothermal kinetics. Many works on non-isothermal kinetics proved that more than one kinetic model of type $d\alpha/dt=A\exp(-E/RT)f(\alpha)$ can describe equally well a given set of non-isothermal experiments. Besides, de Jong et al. have also shown a strong compensation effect between A, E_0 and σ in the distributed activation energy model with Gaussian distribution.[33]

As more and more parameters are assumed to be common during the evaluation, the objective function of the method of least squares (*o.f.* in eq. 1) gets higher and higher values (i.e. the fit worsens), while, on the other hand, the condition of the parameter determination improves.[25,34] One should find a reasonable compromise between the fit quality and the reliability of the parameter values. This way is followed in the present work, too, as illustrated by Table 3. No common parameters were assumed in Evaluation 1; this case corresponds to the separate least squares

evaluation of the six experiments for each sample. In all other evaluations the whole dataset (36 TGA experiments) were evaluated together by the method of least squares.

The assumption of common E_{cell}, E_0, E_{char} values resulted in a slight worsening in *o.f.* When σ was also assumed to be common, *o.f.* remained practically the same. (Cf. evaluations 2 and 3.) The assumption of common E_{cell}, E_0, E_{char}, σ, ν_{cell}, ν_{other}, and ν_{char} in Evaluation 4 resulted only in a slight worsening of *o.f.* in comparison to Evaluations 1 – 3. Evaluation 4 was found to be the most suitable for the purposes of the present work because its parameters retained the characteristic differences between the samples while its favorable N_{param}/N_{exper} ratio (1.5) allowed the reliable determination of its parameters. Its $100\sqrt{o.f.}$ value, 2.46, is only 7% higher than that of Evaluation 1. The results obtained by Evaluation 4 are shown in details in the next paragraph and in the Supporting Information.

When other parameters were assumed to be common instead of ν_{cell}, ν_{other}, and ν_{char}, worse objective function values were obtained for the same number of the unknown parameters, as Evaluations 5, 6 and 7 show in Table 3. In this latter group the mildest worsening of *o.f.* was caused by the assumption of common n_{char} and $f(\alpha_{cell})$ parameters (z and n_{cell}) in Evaluation 5. Hence the assumptions of Evaluations 4 and 5 were combined to achieve a stronger reduction of the number of parameters in Evaluation 8. In this case 10 model parameters were assumed to be common for all samples: E_{cell}, E_0, E_{char}, σ, ν_{cell}, ν_{other}, ν_{char}, z, n_{cell}, and n_{char}; while 5 parameters have different values for the different samples: A_{cell}, A_{other}, A_{char}, y_{other_char}, and c_{cell}. In this evaluation $N_{param}=10+6\times5=40$ parameters were determined from the simultaneous evaluation of 36 experiments, hence N_{param}/N_{exper} is close to 1. However, Evaluation 8 blurs the distinction between the peculiarities of the samples. In this model variant the differences between the samples are expressed by the height and the position of the partial peaks because the parameters determining the shape of these curves (σ, z, n_{cell}, n_{char}) were kept common for all samples. Such approaches may be useful in cases when the reduced computational time and the smaller number of unknown parameters are important.

Table 3: Evaluations with various groups of common model parameters[a]

Evaluation	Common parameters	N_{param}	$\frac{N_{param}}{N_{exper}}$	$100\sqrt{o.f.}$
1	none	6×15	2.5	2.30
2	E_{cell}, E_0, E_{char}	75	2.1	2.40
3	E_{cell}, E_0, E_{char}, σ	70	1.9	2.42
4	E_{cell}, E_0, E_{char}, σ, ν_{cell}, ν_{other}, ν_{char}	55	1.5	2.46
5	E_{cell}, E_0, E_{char}, σ, z, n_{cell}, n_{char}	55	1.5	2.64
6	E_{cell}, E_0, E_{char}, σ, A_{cell}, A_{other}, A_{char}	55	1.5	2.71
7	E_{cell}, E_0, E_{char}, σ, y_{other_char}	65	1.8	3.11
8	E_{cell}, E_0, E_{char}, σ, ν_{cell}, ν_{other}, ν_{char}, z, n_{cell}, n_{char}	40	1.1	2.68

[a] See the Nomenclature for the meaning of the symbols in the Table.

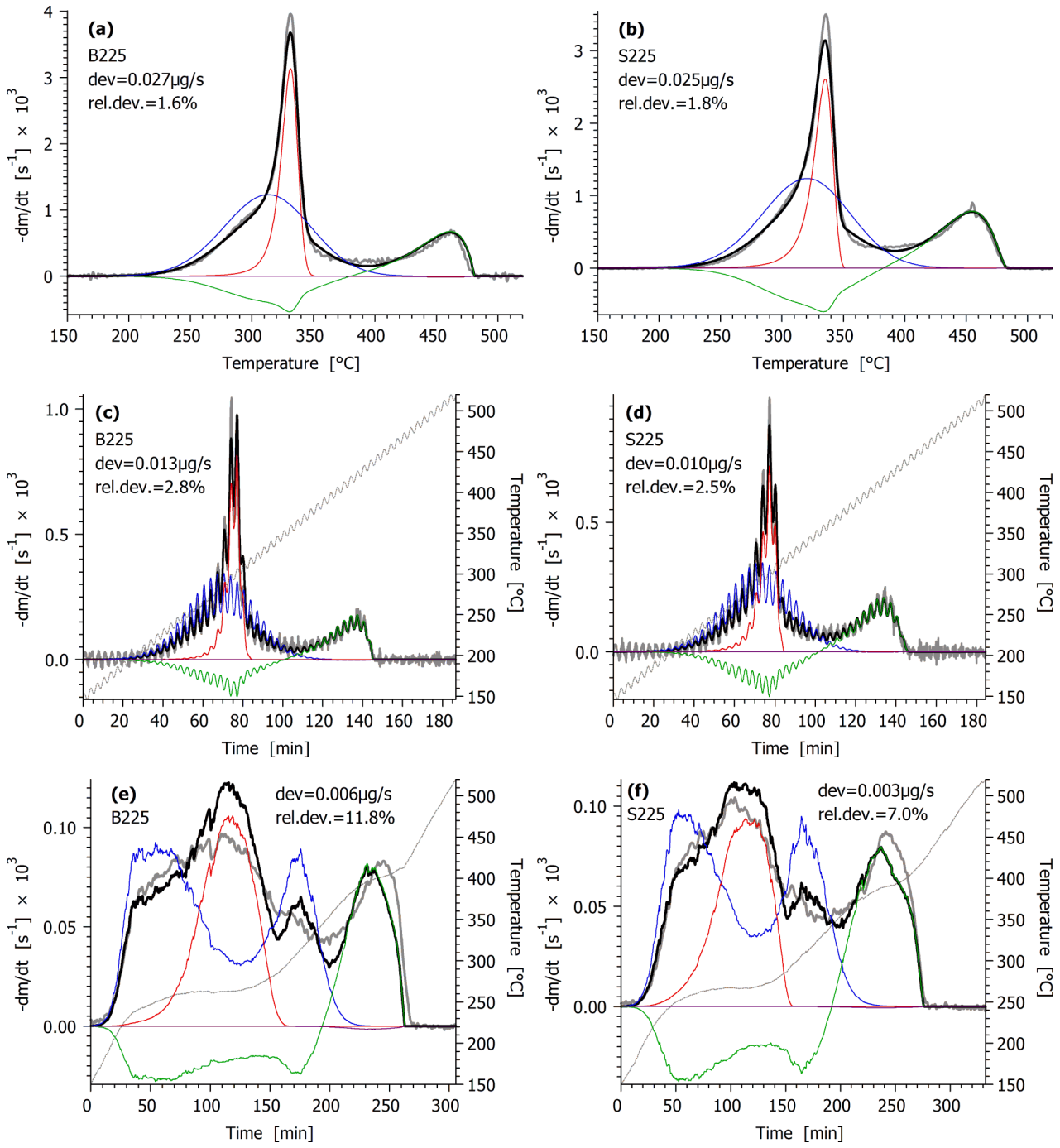

Figure 3. Results of Evaluation 4. The experiments with the samples torrefied at 225°C are shown here at C_{O_2}=0.20. (The complete figure with 36 experiments is shown in the Supporting Information.) Notation: experimental DTG curves normalized by the initial sample mass (gray —); their calculated counterpart (black —); the simulated partial curves: -dm_{cell}/dt (red —); -dm_{other}/dt (blue —); -dm_{char}/dt (green —); -dm_{ash}/dt (purple —); the temperature programs of the modulated and CRR experiments (gray —). In this representation the char formation rate (green line) appears below 0 because mass loss rates (-dm/dt) are plotted.

3.5. Results of Evaluations 4. The fit quality and the partial curves obtained by Evaluation 4 are shown for samples B225 and S225 in Figure 3 at C_{O_2}=0.20. The whole version of Figure 3 with all the 36 experiments is given in the Supporting Information. Table 4 shows the corresponding peak temperatures at 10°C/min and C_{O_2}=0.20. The peak temperature differences between the spruce and the birch samples are also indicated. These differences are small for $d\alpha_{cell}/dt$. The highest difference was observed for $d\alpha_{other}/dt$ between samples S -- and B --. It reflects the DTG differences in the low temperature domain, as shown in Figure 2. (See the shoulder of the green colored curve in Figure 2a.) This difference is smaller between samples S225 and B225 and practically disappears between samples S275 and B275, as the amount of hemicelluloses decreases during the 225°C torrefaction and becomes nearly zero in the 275°C torrefaction. If the peak temperatures of the $d\alpha_{other}/dt$ curves of the torrefied samples are compared to those of the untreated samples, high differences are observed, because the importance of the thermally labile compounds decreases in this pseudocomponent by the torrefaction. The torrefaction at 225°C has negligible effect on the peak temperature of $d\alpha_{cell}/dt$ due to the higher thermal stability of the cellulose. The torrefaction at 275°C, however, markedly decreases the peak temperature of $d\alpha_{cell}/dt$ indicating that the cellulose undergoes some reactions there. The peak temperatures of partial curve $-dm_{char}/dt$ reflect mainly the reactivity differences of the formed char. This value increases with the torrefaction temperature for both samples.

Table 4: Peak temperatures at 10°C/min heating rate in 20% O_2 as obtained by Evaluation 4

	Peak temperature (°C) of		
	$d\alpha_{cell}/dt$	$d\alpha_{other}/dt$	$-dm_{char}/dt$
B ---	335	306	458
S ---	338	316	454
difference[a]	*3*	*10*	*-4*
B225	331	313	461
S225	335	321	455
difference[a]	*4*	*8*	*-6*
B275	322	344	473
S275	327	343	460
difference[a]	*5*	*-1*	*-13*

[a] The difference between the peak temperatures of the spruce and the birch samples.

Table 5 shows how the fit quality depends on the temperature programs of the TGA experiments in Evaluations 4. For this purpose the root mean square deviation and the root mean square relative deviation was calculated for the 10°C/min, modulated and CRR experiments, respectively. The lowest deviation, 0.006 µg/s was obtained for the CRR experiments. The corresponding values of the 10°C/min experiments were 5 times higher. On the other hand, the relative deviation of the 10°C/min experiments were ca. 5 times lower than those of the CRR experiments due to the huge differences in the heights of the corresponding peak maxima, which are also shown in Table 5.

Table 5: Dependence of the deviations and relative deviations on the heating programs in Evaluation 4[a]

Group of experiments	mean DTG peak max.[b] (µg/s)	rms *dev* (µg/s)	rms *rel dev* (%)
linear T(t) 10°C/min	1.35	0.03	2.2
modulated 2°C/min	0.38	0.01	2.8
CRR	0.05	0.06	11.2

[a] The root mean square of the absolute and relative deviations were calculated for the 10°C/min, modulated and CRR experiments, respectively. [b] The averages of the observed DTG peak maxima are given in µg/s.

Table 6 lists the parameters obtained in Evaluations 4. The parameter values obtained in the present work cannot be compared directly to the parameters of the earlier kinetic works on the combustion of torrefied wood due to the high differences in the assumptions, models and evaluation. As an example, let us consider an alternative model that contains first order devolatilization reactions. In first order kinetics the sharpness of a peak depends mainly on the magnitude of the corresponding activation energy. Accordingly, the description of a narrow peak, (i.e. the cellulose decomposition) can be described only by high activation energies while a wide peak can be described by low activation energies. In the present model, however, the width of the cellulose and the non-cellulosic parts were influenced mainly by the $f(\alpha_{cell})$ parameters and σ, respectively. Similar basic differences may arise for other sorts of alternative models, too. Hence the work of Várhegyi et al., 2012,[17] was selected for comparison, where a similar model was employed on a willow sample. The corresponding values are shown in the last column of Table 6. The differences between the results of the two works are not high. The activation energies show only 4 – 9% differences which is less than the activation energy differences reported on pure cellulose in inert atmosphere in a round-robin TGA study.[32] The reaction order of the char bun-off, however, shows a higher alteration. The n_{char} values were 0.58 and 0.64 for the untreated birch and

spruce samples, respectively, while a nearly first order reaction was observed in the earlier work. This might reflect the differences between the samples. The work of Várhegyi et al.[17] used young willow shoots from a Hungarian energy farm with 1.2% ash content while the present work was based on Norwegian forest woods with particularly low ash content. On the other hand, c_{cell} and c_{other} are the same for the untreated birch and for the willow samples of the older work. In the present work the c_{cell} parameters increase with the torrefaction reflecting that the partial devolatilization of the hemicellulose increases the cellulose concentration.

$y_{cell.char}$ had a rather unrealistic value, 0.21, in Várhegyi et al.[17] because the ill definition of this parameter had not been recognised yet there. Similarly, the high values of y_{ash} also appears problematic in the earlier work, while this parameter was determined from the proximate analysis in the present study.

Table 6: Parameters obtained by assuming 7 common parameters [a]

Sample	B --	B225	B275C	S --	S225	S 275	*Means:*	Willow in earlier work [c]
E_{cell} / kJ mol^{-1}	135	=	=	=	=	=	*135*	145
E_0 / kJ mol^{-1}	160	=	=	=	=	=	*160*	166
σ / kJ mol^{-1}	8.1	=	=	=	=	=	*8.1*	11.2
E_{char} / kJ mol^{-1}	153	=	=	=	=	=	*153*	167
ν_{cell}	0.50	=	=	=	=	=	*0.50*	0.61
ν_{other}	0.24	=	=	=	=	=	*0.24*	0.37
ν_{char}	0.47	=	=	=	=	=	*0.47*	0.62
n_{cell}	0.94	0.93	1.23	0.80	0.81	1.06	*0.96*	n.a.
z_{cell}	0.01	0.02	0.03	0.04	0.05	0.04	*0.03*	n.a.
n_{char}	0.58	0.48	0.39	0.64	0.62	0.57	*0.55*	0.95
$\log_{10} A_{cell}$/s^{-1}	9.97	9.99	10.09	9.84	9.86	9.98	*9.95*	10.66
$\log_{10} A_{other}$/s^{-1}	12.44	12.24	11.47	12.16	12.05	11.51	*11.98*	13.04
$\log_{10} A_{char}$/s^{-1}	8.69	8.62	8.50	8.86	8.85	8.80	*8.72*	10.49
y_{other_char}	0.22	0.30	0.51	0.33	0.38	0.55	*0.38*	0.23
c_{cell}	0.30	0.35	0.38	0.30	0.33	0.35	*0.34*	0.30
c_{other}=1- c_{cell}	0.70	0.65	0.62	0.70	0.67	0.65	*0.66*	0.70
$y_{cell.char}$ [c]	0.07	=	=	=	=	=	*0.07*	0.21
y_{ash} [c]	0.01	0.02	0.01	0.01	0.01	0.01	*0.01*	0.20

[a] See Evaluation 4 in Table 3. Character '=' indicates parameter values that are identical in each column. [b] Values obtained in a recent work with a similar model on an untreated willow sample.[17] n_{cell} and z_{cell} are not listed here because the equation for $f(\alpha_{cell})$ was not the same as in the present work. [c] In the present work $y_{cell.char}$ was fixed and y_{ash} was calculated from the ash yield of the proximate analysis (m_{ash}^{anal}), y_{other_char} and $c_{cell,}$ by eq. 12.

The n_{cell} and z parameters together determine $f(\alpha_{cell})$ in equations 9 and 10. Figure 4 shows that the $f(\alpha_{cell})$ curves of the untreated and mildly torrefied samples (lines green and blue) are nearly identical. The torrefaction at 275°C resulted in different $f(\alpha_{cell})$ functions (denoted by red color) indicating that the 275°C torrefaction affects the cellulose reactivity, too. Note that these samples

gave lower peak temperatures for the cellulose decomposition, as mentioned above. (See Table 4.) All $f(\alpha_{cell})$ functions obtained in the present work revealed a strong self-acceleration which is shown by the high increase from the starting values of the $f(\alpha_{cell})$ functions till their peak maxima in Figure 4. Mathematically this is connected to the low values of the z parameters obtained in the least squares evaluation.

The dependence of the char burn-off rate on the normalized amount of char by eq. 6 is shown in Figure 5, where $m_{char}^{n_{char}}$ is plotted as function of m_{char}. Here the layout and the coloring are the same as in Figure 4. In Figure 5 a first order kinetics would give a straight line from coordinates 1,1 to 0,0. The alteration of the obtained curves from the linear indicates a moderate self-acceleration because the burn-off rate of a unit mass of char (the ratio of the *burn-off rate* and m_{char}) is increasing as m_{char} is decreasing. This self-acceleration, however, is much smaller than that of a random-pore kinetics[35] indicating that the internal pore surfaces have only a limited importance in the char burn-off kinetics of these samples.

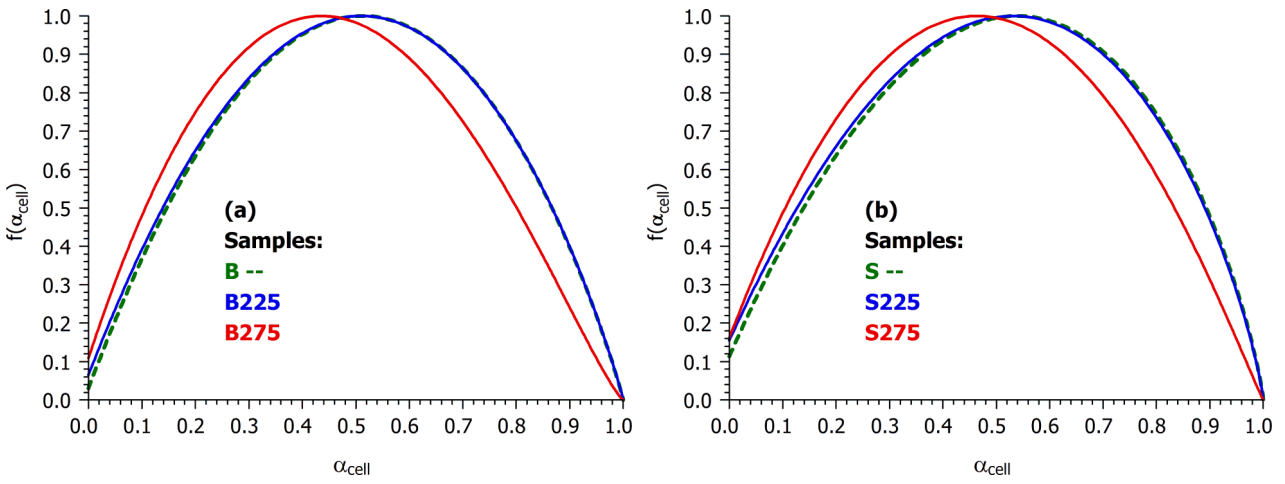

Figure 4. The dependence of the cellulose decomposition rate on the reacted fraction of the cellulose in Evaluation 4. $f(\alpha_{cell})$ is plotted as function of α_{cell}. The corresponding parameter values are listed in Table 6.

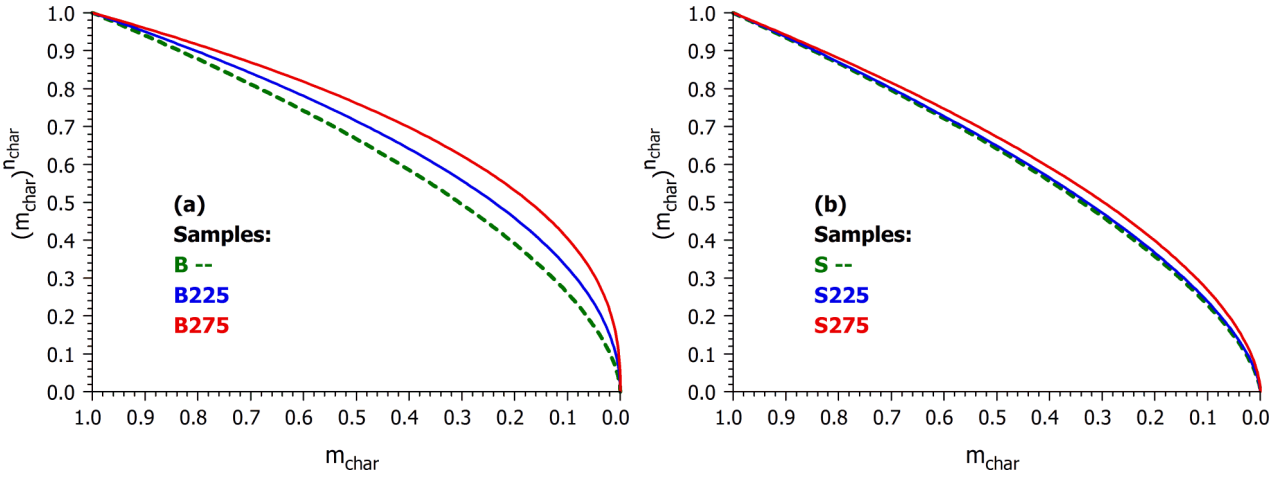

Figure 5. The dependence of the char burn-off rate on the normalized amount of char by eq. 6 in Evaluation 4. $m_{char}^{n_{char}}$ is plotted as function of m_{char}. The corresponding parameter values are listed in Table 6

4. CONCLUSIONS

(1) The combustion of four torrefied wood samples and their feedstocks (a deciduous and an evergreen species) was studied at slow heating programs, under well-defined conditions. Particularly low sample masses were employed to avoid the self-heating of the samples due to the huge reaction heat of the combustion. Six TGA experiments were carried out for each sample with three different temperature programs in 5 and 20% O_2, respectively. Strongly different temperature programs were selected to increase the information content available for the modeling: linear, modulated and constant-reaction rate (CRR) temperature programs. The ratio of the highest and lowest peak maxima was around 50 in the set of the experiments used for the evaluation. In this way the obtained models described the experiments in a wide range of experimental conditions.

(2) A recent combustion model consisting of two devolatilization reactions and a successive char burn-off reaction was employed with a minor modification. The cellulose decomposition in the

presence of oxygen was described by a model that had two adjustable parameters to mimic self-acceleration tendencies. The decomposition of the non-cellulosic parts of the biomass was described by a distributed activation model. The char burn-off was approximated by power-law (n-order) kinetics. Each of these reactions had its own dependence on the oxygen concentration that was also expressed by power-law kinetics. This model was tested earlier on one wood sample (willow), hence the present work is a further step to gain experience with its applicability. The reliability of the model and the obtained parameters was improved by decreasing the number of the parameters and by clarifying a compensation effect problem.

(3) The complexity of the applied model reflects the complexity of the studied materials. The fast developing rate of the computers will allow the use of complex kinetic submodels in actual industrial simulations, too. Presently a medium-priced desktop computer can calculate one million -dm/dt curves by this model within ca. 1.5 hours at the highly irregular T(t) functions of the present study.

(4) The employed model contains 15 unknown parameters for a given biomass. The relatively wide range of experiments made possible the determination of so many parameters by the method of least squares. The torrefaction have some impact on the parameters, especially on the ones describing the devolatilization of the hemicelluloses and other thermally labile parts of a biomass sample. These parts decompose more or less during the torrefaction, as the corresponding c_{cell} and c_{other}=1- c_{cell} parameters indicated. The cellulose reactivity was also affected at the higher torrefaction temperature, 275°C, of the study.

(5) Part of the kinetic parameters could be assumed common for the six samples without a substantial worsening of the fit quality. This approach increased the average experimental information for an unknown parameter and revealed the similarities in the behavior of the different samples. The following kinetic parameters could be assumed identical for the six samples with only a slight worsening of the fit quality: the activation energies; the mean and the width of the

activation energy distribution in the DAEM part of the model and the dependence of the reactions on the oxygen concentration.

ASSOCIATED CONTENT

Supporting Information.

The results of Evaluation 4 are shown in figures including all the 36 experiments. This material is available free of charge via the Internet at http://pubs.acs.org.

AUTHOR INFORMATION

Corresponding Author

* To whom correspondence should be addressed. E-mail: varhegyi.gabor@ttk.mta.hu, Tel. +36 1 4381148, Fax: +36 1 4381147

ACKNOWLEDGMENT

The authors acknowledge the financial support by the Research Council of Norway and a number of industrial partners through the project STOP ("STable OPerating conditions for biomass combustion plants"). STOP is also a part of the research center CenBio (Bioenergy Innovation Centre). G.V. is grateful for the support of the Hungarian National Research Fund (OTKA K72710).

APPENDIX: Compensation effect between three model parameters

As outlined in Section 3.4 there is a strong compensation effect between parameters $y_{cell.char}$, c_{cell} and y_{other_char}. The problem will be shown here for the behavior of the untreated spruce sample (S --). Figure 6 shows the corresponding linear heating rate experiments from Evaluation 1. It is worth observing that the rate of the char burn-off becomes higher than the rate of the char formation between 380 and 390°C. Note that mass loss rates were plotted; hence the dominance of the char

burn-off is indicated by the positive values of the overall char mass loss rate (green curve). Most of the devolatilization is accomplished till this temperature; only a small portion of the non-cellulosic part of the sample (line blue) decomposes above ca. 380°C.

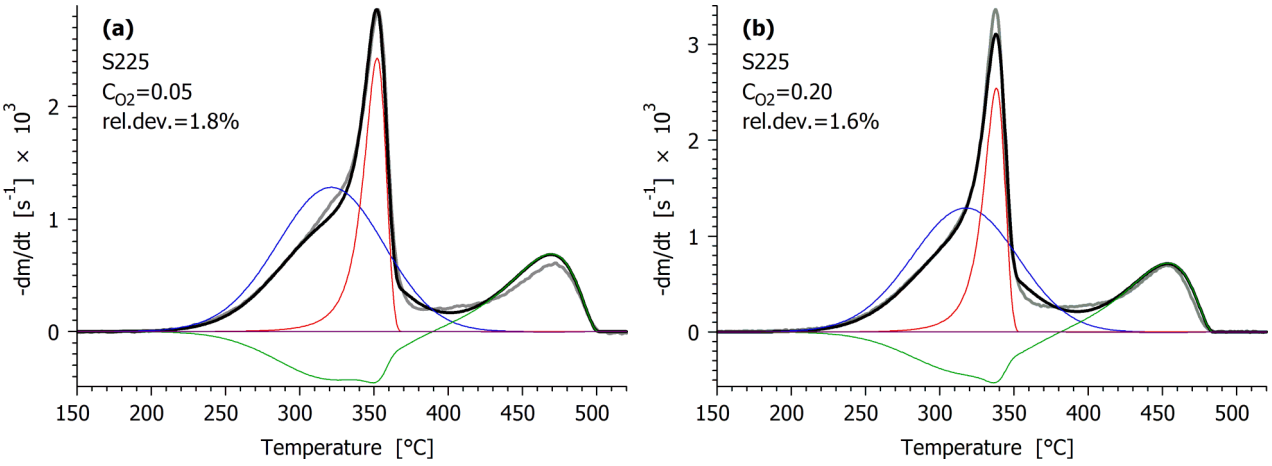

Figure 6. The linear heating rate experiments of the untreated spruce sample in Evaluation 1. (See Figure 3 for the notations).

The mass loss of the devolatilization depends on the amount of volatiles formed from the two pseudo-components. Keeping in mind the definitions of the *c* and *y* parameters and eq. 5c, we get:

normalized mass loss rate of devolatilization =

$$c_{cell}\ (1-y_{cell.char})\ \frac{d\alpha_{cell}}{dt} + (1-c_{cell})\ (1-y_{other\_char})\ \frac{d\alpha_{other}}{dt} \qquad (13)$$

Any $y_{cell.char}$, c_{cell} and y_{other_char} combination gives exactly the same mass loss rate in eq. 13 as far as the values of the coefficients, $c_{cell}\ (1-y_{cell.char})$ and $(1-c_{cell})\ (1-y_{other\_char})$ do not change.

The normalized amount of char formed from the devolatilization is

$$c_{cell}\, y_{cell.char} + (1-c_{cell})\, y_{other\_char} \qquad (14)$$

Most of the amount defined by eq. 14 forms before the start of the char burn-off while a small portion is produced around ca. 380 – 420°C, where the devolatilization of the non-cellulosic part of the sample terminates. The ratio of these amounts, however, has only a limited importance on the overall kinetics because the char burn-off occurs mainly above 420°C, as the green curves show in

Figure 6. If $y_{cell.char}$, c_{cell} and y_{other_char} vary so that neither the devolatilization kinetics (eq. 13) nor the amount of formed char (eq. 14) change then the variation affects only the ratio of the amounts of char formed before the char burn-off and simultaneously with the char burn-off.

As an illustration, the untreated spruce experiments were evaluated so that $y_{cell.char}$ got fixed values (0, 0.1, 0.2, 0.3 and 0.4) while c_{cell} and y_{other_char} were determined from the experimental data by the method of least squares. In this test all other model parameters were kept constant at the values obtained in Evaluation 1. The results are shown in Table 7. Note that $100\sqrt{o.f.}$ was 2.127 in for sample S -- in Evaluation 1. As the last row of Table 7 indicates, only the third digit of its value changed at higher $y_{cell.char}$. The normalized amount of the formed char, $c_{cell}\, y_{cell.char} + (1\text{-}c_{cell})\,(1\text{-}\, y_{other\_char})$ also shows similarly small changes. On the other hand, c_{cell} and y_{other_char} change markedly to keep the values of the rest of the table constant or nearly constant.

Table 7: Least squares determination of c_{cell} and y_{other_char} at various values of $y_{cell.char}$ by the evaluation of the untreated spruce experiments[a]

$y_{cell.char}$	0	0.1	0.2	0.3	0.4
c_{cell}	0.285	0.316	0.356	0.407	0.475
y_{other_char}	0.346	0.316	0.274	0.212	0.110
$c_{cell}\,(1\text{-}\, y_{cell.char})$	0.285	0.285	0.285	0.285	0.285
$(1\text{-}c_{cell})\,(1\text{-}\, y_{other\_char})$	0.468	0.468	0.468	0.468	0.468
$c_{cell}\, y_{cell.char} + (1\text{-}c_{cell})\,(1\text{-}\, y_{other\_char})$	0.247	0.247	0.247	0.248	0.248
$100\sqrt{o.f.}$	2.127	2.127	2.127	2.128	2.129

[a] The values of all other parameters were taken from Evaluation 1 and were not changed.

NOMENCLATURE

α = reacted fraction of a component or pseudocomponent (dimensionless)

ν = reaction order with respect of oxygen concentration

σ = width parameter (variance) of Gaussian distribution (kJ/mol)

A = pre-exponential factor (s^{-1})

C_{O_2} = V/V concentration of the ambient oxygen (dimensionless)

dev = root mean square of the deviations between the observed and calculated values of a DTG curve (μg/s)

E = activation energy (kJ/mol) or mean activation energy in a distributed activation energy model (kJ/mol)

f = empirical function (eq. 10) expressing the change of the reactivity as the reactions proceed (dimensionless)

h_k = either the height of an experimental curve (s^{-1}) or 5×10^{-4} s^{-1}, whichever is higher

m = the mass of the sample or a component of the sample normalized by the initial sample mass (dimensionless)

m_{ash}^{anal} = 1/100th of the total ash determined by proximate analysis (dimensionless)

n = reaction order (dimensionless)

o.f. = the objective function minimized in the least squares evaluation (dimensionless)

N_{exper} = number of experiments evaluated together by the method of least squares

N_k = number of evaluated data on the kth experimental curve

N_{param} = number of parameters determined in the evaluation of a series of experiments

R = gas constant (8.3143×10^{-3} kJ mol^{-1} K^{-1})

rel.dev = the deviation (*dev*) expressed as per cent of the corresponding peak height

t = time (s)

T = temperature (°C, K)

y = yield (dimensionless). $y_{cell.char}$ and y_{other_char} represent the char yield from the cellulose and from the rest of the biomass, respectively. y_{ash} denotes the ash yield from char

z = formal parameter in eq. 10 (dimensionless)

Subscripts:

cell = cellulose

i = digitized point on an experimental curve

k = experiment

other = non-cellulosic organic biomass constituents

ur = unreacted sample

REFERENCES

1. Faaij, A. P. C. *Energy Policy* **2006,** 34, (3), 322-342.

2. World Energy Outlook 2009, International Energy Agency, Paris, France, 2009. Available at http://www.iea.org/publications/freepublications/publication/weo2009.pdf .

3. van der Stelt, M. J. C.; Gerhauser, H.; Kiel, J. H. A.; Ptasinski, K. J. *Biomass Bioenergy* **2011**, 35, 3748-3762.

4. Tapasvi, D. T., K-Q.; Wang, L.; Skreiberg, Ø.; Khalil, R. *Proceedings of the 9th European Conference on Industrial Furnaces and Boilers, Estoril, Portugal* **2011**, (ISBN 978-972-99309-6-6).

5. Tapasvi, D.; Khalil, R. A.; Skreiberg, Ø.; Tran, K.-Q.; Gronli, M. G. *Energy Fuels* **2012**, *26*, 5232–5240.

6. Zheng, A.; Zhao, Z.; Chang, S.; Huang, Z.; He, F.; Li, H. *Energy Fuels* **2012,** *26*, 2968-2974.

7. Wannapeera, J.; Fungtammasan, B.; Worasuwannarak, N. *J. Anal. Appl. Pyrolysis* **2011,** *92*, 99-105.

8. Prins, M. J.; Ptasinski, K. J.; Janssen, F. J. J. G. *Energy* **2006,** 31, 3458-3470.

9. Pimchuai, A.; Dutta, A.; Basu, P. *Energy Fuels* **2010,** 24, 4638-4645.

10. Jones, J. M.; Bridgeman, T. G.; Darvell, L. I.; Gudka, B.; Saddawi, A.; Williams, A. *Fuel Proc. Tech.* **2012,** 101, 1-9.

11. Couhert, C.; Salvador, S.; Commandré, J. M. *Fuel* **2009,** 88, 2286-2290.

12. Broström, M.; Nordin, A.; Pommer, L.; Branca, C.; Di Blasi, C. *J. Anal. Appl. Pyrolysis* **2012,** 96, 100-109.

13. Bridgeman, T. G.; Jones, J. M.; Shield, I.; Williams, P. T. *Fuel* **2008,** 87, 844-856.

14. Arias, B.; Pevida, C.; Fermoso, J.; Plaza, M. G.; Rubiera, F.; Pis, J. J. *Fuel Proc. Tech.* **2008,** 89, 169-175.

15. Di Blasi, C. *Prog. Energy Combust. Sci* **2008,** 34, 47-90.

16. Di Blasi, C. *Prog. Energy Combust. Sci.* **2009,** *35*, 121-140.

17. Várhegyi, G.; Sebestyén, Z.; Czégény, Z.; Lezsovits, F.; Könczöl, S. *Energy Fuels* **2012,** *26*, 1323-1335.

18. High resolution thermogravemetric analysis - A new technique for obtaining superior analytical results. TA Instruments report TA-023. Available at: http://www.tainstruments.co.jp/application/pdf/Thermal_Library/Applications_Briefs/TA023.PDF

19. Várhegyi, G. *J. Anal. Appl. Pyrolysis* **2007**, *79*, 278-288.

20. Becidan, M.; Várhegyi, G.; Hustad, J. E.; Skreiberg, Ø. *Ind. Eng. Chem. Res.* **2007**, *46*, 2428-2437.

21. Várhegyi, G.; Czégény, Zs.; Liu, C.; McAdam, K. *Ind. Eng. Chem. Res.,* **2010**, *49*, 1591-1599.

22. Várhegyi, G.; Till, F. *Thermochim. Acta* **1999**, *329*, 141-145.

23. Várhegyi, G.; Chen, H.; Godoy, S. *Energy Fuels* **2009**, *23*, 646-652.

24. Várhegyi, G.; Szabó, P.; Mok W. S. L., Antal, M. J., Jr. *J. Anal. Appl. Pyrolysis* **1993**, *26*, 159-174.

25. Várhegyi, G.; Bobály, B.; Jakab, E.; Chen, H. *Energy Fuels,* **2011**, *25,* 24-32.

26. Werkelin, J.; Skrifvars, B.-J.; Zevenhoven, M.; Holmbom, B.; Hupa M. *Fuel* **2010**, *89*, 481-493

27. Conesa, J. A.; Caballero, J. A.; Marcilla, A.; Font, R. *Thermochim. Acta* **1995**, *254*, 175–192.

28. Capart, R.; Khezami, L.; Burnham, A. K. *Thermochim. Acta* **2004**, 417, 79–89.

29. Várhegyi, G.; Szabó, P.; Jakab, E.; Till, F.; Richard J-R. *Energy Fuels* **1996**, *10*, 1208-1214.

30. Várhegyi, G.; Pöppl, L.; Földvári, I. *Thermochim. Acta* **2003**, *399*, 225-239.

31. Donskoi, E.; McElwain, D. L. S. *Combust. Flame* **2000**, *122*, 359-367.

32. Grønli, M.; Antal, M. J., Jr.; Várhegyi, G. *Ind. Eng. Chem. Res.* **1999**, *38*, 2238-2244.

33. de Jong, W.; Di Nola, G.; Venneker, B. C. H.; Spliethoff, H.; Wójtowicz, M. A. *Fuel,* **2007**, *86*, 2367-2376.

34. Várhegyi, G.; Czégény, Zs.; Jakab, E.; McAdam, K.; Liu, C. *J. Anal. Appl. Pyrolysis* **2009**, *86*, 310-322.

35. Gavalas, G. R. *AIChE J.* **1980**, *26*, 577-585.

LIST OF FIGURE CAPTIONS

Figure 1. Temperature programs used in the TGA experiments. Note that each of the twelve constant heating rate experiments has different T(t); this figure shows four of them.

Figure 2. Comparison of the experiments at 10°C/min heating rate, in 20% oxygen

Figure 3. Results of Evaluation 8. The experiments with the samples torrefied at 225°C are shown here at C_{O_2}=0.20. (The complete figure with 36 experiments is shown in the Supporting Information.) Notation: experimental DTG curves normalized by the initial sample mass (gray —); their calculated counterpart (black ━); the simulated partial curves: -dm_{cell}/dt (red —); -dm_{other}/dt (blue —); -dm_{char}/dt (green —); -dm_{ash}/dt (magenta —); the temperature programs of the modulated and CRR experiments (gray —). In this representation the char formation rate (green line) appears below 0 because mass loss rates (-dm/dt) are plotted.

Figure 4. The dependence of the cellulose decomposition rate on the reacted fraction of the cellulose by equations 9 and 10. $f(\alpha_{cell})$ is plotted as function of α_{cell}. Figures 4**a** and 4**b** are the results of the separate evaluation of the six experiments on each sample (Evaluation 1)**;** while the curve in Figure 4**c** was obtained by the simultaneous evaluation of 36 experiments assuming 10 model parameters to be common for the six samples (Evaluation 8). The corresponding parameter values are listed in Tables 6 and 7.

Figure 5. The dependence of the char burn-off rate on the normalized amount of char by eq. 6. $m_{char}^{n_{char}}$ is plotted as function of m_{char}. Figures 5**a** and 5**b** are the results of the separate evaluation of the six experiments on each sample (Evaluation 1)**;** while the curve in Figure 5**c** was obtained by the simultaneous evaluation of 36 experiments assuming 10 model parameters to be common for the six samples (Evaluation 8). The corresponding parameter values are listed in Tables 6 and 7.

Figure 6. The linear heating rate experiments of the untreated spruce sample in Evaluation 1. (See Figure 3 for the notations).